INTERNATIONAL JOURNAL OF AUTOMOTIVE AND MECHANICAL ENGINEERING
ISSN: 2229-8649 e-ISSN: 2180-1606
VOLUME 22, ISSUE 3, 2025, 12627 - 12639
DOI: https://doi.org/10.15282/ijame.22.3.2025.8.0965

RESEARCH ARTICLE

CFD Analysis of Patient-Specific and Idealized Models for Predicting Stenosis Locations and Hemodynamic Disturbances in Peripheral Arterial Disease

Ukasyah Zulfaqar Shahrulakmar[1], Nasrul Hadi Johari[1,2]*, Chandran Nadarajan[3], Baolei Guo[4]

[1]Faculty of Mechanical and Automotive Engineering Technology, Universiti Malaysia Pahang Al-Sultan Abdullah, 26600 Pekan, Pahang, Malaysia
[2]Centre for Advanced Industrial Technology, Universiti Malaysia Pahang Al-Sultan Abdullah, 26600 Pekan, Pahang, Malaysia
[3]Department of Radiology, School of Medical Sciences, Universiti Sains Malaysia, Kubang Kerian, 16150 Kota Bharu, Kelantan, Malaysia
[4]Department of Vascular Surgery, Institute of Vascular Surgery, Zhongshan Hospital, Fudan University, Shanghai, China

ABSTRACT – Peripheral arterial disease (PAD), a condition caused by atherosclerosis, poses significant cardiovascular risks by disrupting blood flow. Computational fluid dynamics offers insights into vascular remodeling mechanisms, leveraging patient-specific anatomical data from computed tomography angiography (CTA) to enhance the accuracy of blood flow analysis. This study aims to evaluate the capability of an idealized arterial model in simulating hemodynamic parameters and blood flow patterns by comparing it with patient-specific geometries. Additionally, the study investigates the impact of stenosis at different locations within the femoral artery: upstream, downstream, and at the Profunda on flow disturbances and downstream regions. Blood flow was modeled as a Newtonian fluid, assuming a constant viscosity independent of shear rate, which is a reasonable approximation for femoral arteries where shear rates are typically high. Both an idealized PAD geometry and a patient-specific model derived from CTA data were employed for simulations. Results showed elevated blood velocities at bifurcations, notably at the superficial femoral artery (SFA) and profunda femoral artery, with peak velocities exceeding 1.90 m/s. Regions of low wall shear stress (WSS) were identified at key branching points and along arteries such as the popliteal and tibial arteries. The idealized model effectively replicated patient-specific flow patterns. Upstream stenosis caused severe flow disturbances, with velocities up to 3.9 m/s and Reynolds numbers (Re) of 1272 in the mainstream region, disrupting flow recovery. Downstream stenosis caused severe disturbances, with Re of 1835 beyond the bifurcations, whereas profunda stenosis had minimal effect, maintaining Re below 1000. This study emphasizes the importance of patient-specific anatomical factors in predicting stenosis and highlights the utility of idealized models for generating hemodynamic profiles. These findings enhance the pre-treatment planning and management methods for PAD patients.

ARTICLE HISTORY
Received : 31st Dec. 2024
Revised : 24th Apr. 2025
Accepted : 15th July 2025
Published : 01st Sept. 2025

KEYWORDS
Peripheral arterial disease
Computational fluid dynamics
Atherosclerosis
Femoral artery
Idealized arterial geometry

1. INTRODUCTION

Peripheral Arterial Disease (PAD) is a common and serious heart disease that blocks blood flow in the arteries of the lower extremities, mostly because of atherosclerosis. As of 2020, PAD has affected about 200 million people around the world [1]-[3]. The condition is especially worrisome because it raises the risk of serious heart problems, such as heart attack, transient ischaemic attack, and stroke. Several well-known risk factors such as diabetes mellitus, smoking, high blood pressure, dyslipidaemia, and having heart disease beforehand, are closely related to the pathophysiology of PAD [4]-[5]. One of the most significant issues with PAD is that it often starts slowly, and many patients do not exhibit any symptoms for a period of time. However, a large group of people have intermittent claudication, which is a common symptom that causes pain and cramps in the lower limbs during activity and usually goes away with rest. PAD can get worse and lead to more serious ischaemic conditions if it isn't treated quickly and correctly. This can cause problems like chronic leg ulcers, gangrene, and even amputation of the limb in the worst cases [6].

PAD is primarily caused by atherosclerotic plaque formation inside artery walls, which results in progressive narrowing of the lumen and restricted blood flow. This process mostly affects the lower limb arteries, notably the profunda femoris and external iliac arteries, where plaque deposition causes considerable hemodynamic dysfunction [6]. Its gradual progressive nature emphasizes the importance of early detection and extensive management techniques to reduce the potential of severe outcomes. Invasive diagnostic approaches that combine geometric features and hemodynamic measures are commonly used to assess plaque formation and severity within arteries. Understanding the development of arterial stenosis requires the use of key hemodynamic markers such as flow patterns, wall shear stress (WSS), and pressure distribution [7]-[8]. A decrease in WSS, particularly in specific arterial areas, has been associated with plaque development because it can influence the regulation of genes, resulting in arterial constriction and increased vascular stiffness [2], [9]-[10]. In severe stenosis, disturbed blood flow may change from a laminar to a turbulent condition, increasing the risk of plaque rupture and subsequent thrombosis [11].

*CORRESPONDING AUTHOR | N.H Johari | ✉ nhadi@umpsa.edu.my

Computational fluid dynamics (CFD) has appeared as a helpful tool for exploring arterial haemodynamics and the basic principles of arterial remodelling, particularly in atherosclerosis and stenosis [2], [11]-[13]. Despite tremendous progress in CFD applications, there are significant gaps in our understanding of vascular illnesses and the complexity of blood flow dynamics in instances of PAD [2], [6], [14]-[21]. Many present computational studies have mostly focused on the influence of stenting and the phenomena of restenosis, with less emphasis given to the early phases of stenosis development in the peripheral arteries (PA) of the lower limbs [11], [16], [18], [20]-[22]. Furthermore, research addressing plaque formation and flow behavior within peripheral arteries often varies in the standardization of arterial diameter and length, frequently concentrating on specific arterial segments [6], [23]-[27]. While extensive research has been conducted on major arteries such as the coronary and carotid arteries, peripheral arteries have not received the same level of attention. This lack of focus has resulted in an absence of a cohesive framework for comprehensively understanding the effects of plaque throughout the entire peripheral arterial system [15], [28]-[33].

CFD modelling of blood flow dynamics in PAD patients has primarily focused on bifurcation zones, where large changes in WSS are most evident. While idealized models make the computational process easier, they frequently fail to adequately represent patient-specific situations. As a result, the complex relationship between geometric characteristics and WSS alterations is still poorly understood, limiting the ability to precisely identify stenosis locations and their broader impact on the peripheral arterial system, particularly in the narrower downstream regions. Despite advances in computational modelling of vascular illnesses, there is still a noticeable gap in research that includes patient-specific geometry of peripheral arteries, particularly for PAD cases affecting the superficial femoral artery (SFA). Prior research has frequently relied on idealized models or focused on bifurcation zones and stent assessments, which may not fully capture the hemodynamic complications caused by anatomical diversity and plaque-induced stenosis in peripheral arteries. The current study explicitly addresses this gap by merging an idealized and patient-specific model built from a computed tomography angiography (CTA) dataset of a PAD patient, allowing for a direct comparison of hemodynamic behaviours under physiologically relevant situations. This dual-model approach allows for a better understanding of how geometric irregularities influence wall shear stress and flow separation, contributing to more accurate evaluations of PAD progression and providing a foundation for patient-tailored diagnosis and treatment planning [18], [20]-[21].

2. METHODS AND MATERIALS

The method used in this research is structured in multiple phases to allow for a thorough examination of hemodynamic behaviour in PA. The initial phase is creating a generalised idealized geometry of a healthy PA. This step establishes a baseline for future comparisons and analysis [34]. Upon constructing the idealized models, the next phase is to recreate patient-specific femoral artery (FA) geometry. This is carried out using a medical image processing technology and data collected via CTA. These reconstructed models serve as the foundation for the initial CFD simulations, which seek to depict the complexity of blood flow inside the patient's particular vascular architecture. The study then continues on to a comparative analysis, in which the fidelity of patient-specific models in duplicating real femoral artery blood flow is compared to idealized models. This comparison is crucial for evaluating the correctness of the patient-specific simulations as well as understanding the limitations of idealized models in capturing the complex flow dynamics found in real physiological circumstances.

Finally, the study investigates changes in flow behaviour within the femoral artery by analyzing various stenosis locations, with a particular emphasis on the mid-superficial femoral artery (L1), proximal to the adductor canal (L2), and profunda (L3) areas. This part of the technique provides insights into how stenosis at different locations affects overall hemodynamic patterns, possibly altering the progression of atherosclerosis and the effectiveness of therapeutic interventions.

2.1 Geometry Reconstruction

Two geometric models were reconstructed for this study, an idealized model and a patient-specific model, as previously mentioned. In order to simplify the geometry and preserve the standard dimensions and significant geometric properties, the idealized model was created using SolidWorks 2020 (Dassault Systems, Velizy, France) software, which deliberately removed artery curvature and inadequate physiological irregularities. The idealized model comprises a length of 200 mm and extends from the FA with a proximal diameter of 6 mm to the adductor canal region, which narrows to 5 mm - dimensions that are entirely based on the appropriate patient model. In contrast, the patient-specific model was a realistic 3D reconstruction based on DICOM-format CTA scans of a 58-year-old Asian male with PAD. The Human Research Ethics Committee of Universiti Sains Malaysia (USM/JEPeM/22020100) authorised the usage of this patient data. Figure 1 shows that the CTA data revealed an aberrant constriction in the mid-segment of the SFA. CT scans (512 × 512 pixels, 1 mm slice thickness, 1 mm interslice distance) were processed using 3D Slicer software to extract vascular anatomy. An acknowledged radiologist at HUSM visually inspected the CTA information and designated the contralateral artery as the "healthy" model. Non-essential anatomical components were removed, and the surfaces were smoothed using Autodesk Meshmixer to reduce surface roughness and eliminate faulty wall characteristics, in accordance with standard practices [35]-[36]. Meshmixer was chosen primarily for its ability to increase mesh quality by decreasing noise and ensuring smooth, clean wall surfaces, which is a critical factor in producing accurate CFD simulation results since surface anomalies can cause computational errors. The improved model was saved in ASCII STL format, and the number of faces was further reduced using SolidWorks 2020. SolidWorks was chosen for its ability to optimise and simplify complex

geometries while preserving important anatomical characteristics. This step significantly improved computational efficiency by reducing mesh complexity without compromising model fidelity. Both 3D Slicer and SolidWorks are widely accepted tools in both engineering and medical modelling domains, ensuring reliable preparation of geometries for CFD simulation.

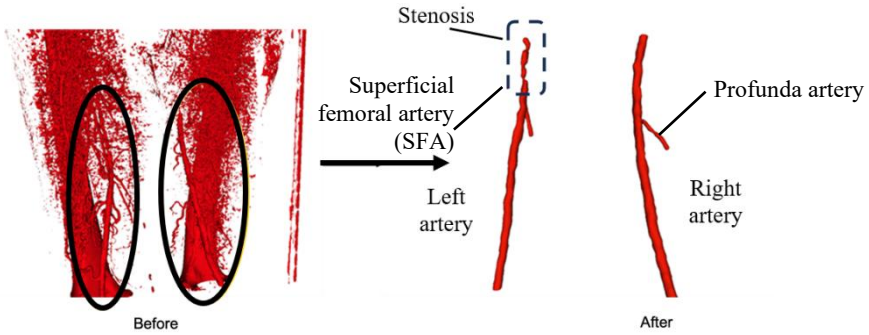

Figure 1. Anatomically realistic three-dimensional (3D) model of the femoral artery (FA) extracted from CT images. The left artery exhibits a stenotic shape at the location proximal to the bifurcation, while the contralateral artery (right artery) represents healthy vascular geometry

2.2 Region of Interest of Study for Three Different Stenosis Locations

The reconstructed stenotic FA has undergone modifications with two more stenosis locations in order to examine the impact of various stenosis locations surrounding the bifurcation area. Hence, three geometries with different stenosis locations, i.e., the original reconstructed stenotic FA (L1) is at mid-superficial femoral artery, proximal to the adductor canal. The fabricated stenosis (L2) is at the downstream of the bifurcation of the FA, and the L3 is at the profunda artery, as highlighted in Figure 2. All geometries are in the region of interest, spanning approximately 30 mm around the bifurcation area. The size of the stenosis is maintained at 75% of its nominal diameter.

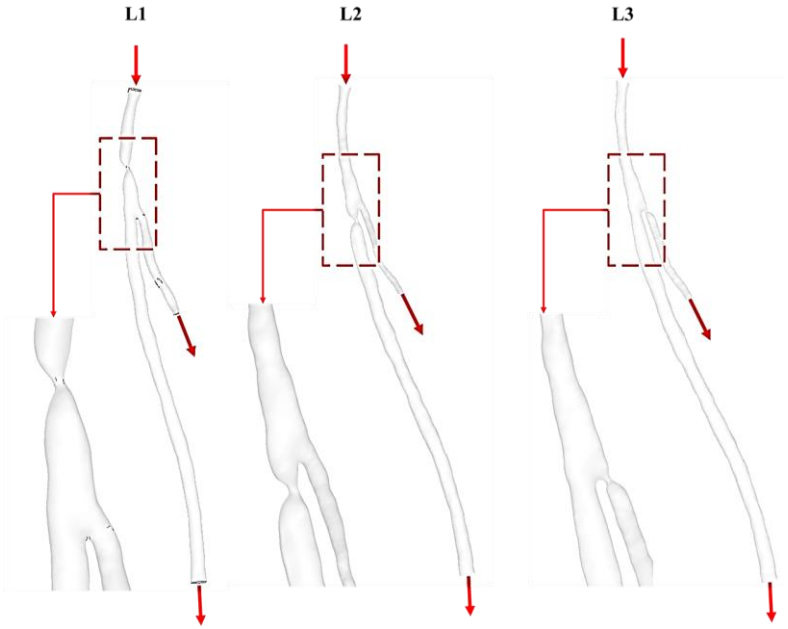

Figure 2. Region of interest for flow analysis in different stenosis locations. L1: upstream stenosis model; L2: downstream stenosis model; L3: Profunda stenosis model

2.3 Mesh Generation

The PAD model geometries were exported to ANSYS Workbench (ANSYS Inc., Canonsburg, PA, USA) for mesh generation, which required both global and local meshing due to the geometry's complexity. ANSYS Mesher was employed to create a refined tetrahedral mesh [37]-[39], with prism mesh layers near the wall comprising seven layers with the first layer thickness of 0.025 mm to capture flow accurately [40]-[41]. A tetrahedral mesh was selected for this study because it offers excellent adaptability to irregular and patient-specific vascular geometries, particularly around bifurcations, stenoses, and curved regions. Compared to structured hexahedral meshes, tetrahedral meshes require less manual intervention and are capable of generating smooth transitions around sharp geometrical features, making them suitable for complex arterial models. The advanced sizing function for proximity and curvature was employed, along with high-level smoothing and a slower transition angle [42]. For patient-specific geometries, similar meshing parameters were applied, with element sizes of 0.50, 0.35, 0.25, and 0.20 mm, a mesh sensitivity analysis was carried out [40]. For

consistency and computational efficiency, an element size of 0.25 mm was selected globally. The independent mesh in the healthy model has a number of elements of 2.17 million and 473 thousand nodes, whereas the patient-specific healthy model has 2.2 million elements and 477 thousand nodes. The outcome won't be influenced by additional element refinement. Thus, this element size will also reduce the computational cost and period subsequently. This element size provided stable results, and further refinement did not significantly influence the outcome, reducing computational cost and time.

2.4 Boundary Conditions and Model Parameters

The transient and incompressible blood flow in the healthy and stenosed FA models was intended to imitate physiologically realistic blood flow, mirroring Newtonian blood flow in larger arteries such as the carotid, peripheral, and aortic segments. ANSYS FLUENT 21.0 (ANSYS Inc., Canonsburg, PA, USA) was used to simulate the blood flow condition inside the artery. The density of 1060 kg/m³ and viscosity of 3.5×10^{-3} kg/ms, blood is a non-Newtonian fluid that behaves like a Newtonian fluid under high strain rates. In this study, transient laminar flow was applied to both the idealized and patient-specific healthy artery models (Figure 3). A pulsatile velocity waveform based on femoral artery flow from Olufsen et al. was used to define the inlet boundary condition [43] representing a typical cardiac cycle duration of 0.8 seconds. This decision was based on the fact that under normal physiological conditions, blood flow in large arteries typically remains laminar due to relatively low Reynolds numbers (generally < 2300), especially in the absence of pathological narrowing. The presence of arterial stenosis results in significant geometric narrowing, which causes local flow acceleration, high shear gradients, and disturbed flow downstream. These conditions can lead to flow transition and, in severe cases, localized turbulence. The SST-Trans model was chosen because it effectively captures both the onset of laminar-to-turbulent transition and the fully developed turbulent regions, especially in complex vascular geometries [44]. This modeling choice was validated by comparing simulation results with the experimental benchmark data from Ahmed and Giddens. The SST-Trans model outperformed the conventional k-ε model used in the study by N.H. Johari by providing velocity profiles and recirculation zones that matched experimental flow patterns [41]. Additionally, the SST-Tran simulations' consumption conditions used a turbulence intensity (TI) of 1.5%, which is within the typical range for physiological arterial flow conditions and matches values from previous CFD studies [45]-[46].

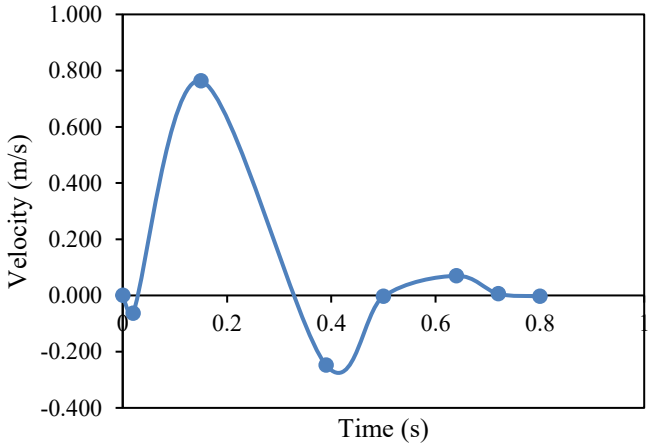

Figure 3. Reconstructed time-dependent inlet velocity waveform [47]

Rigid walls with non-slip conditions were assumed in the simulations [20], [48]. Due to these presumptions, the simulation's wall possessed zero velocity components. This presumption ensures that the velocity variables at the wall are zero. In order to simplify the model and reduce computational complexity, numerous CFD models of arterial flow assume rigid artery walls. This assumption is appropriate for this study, which focuses on hemodynamics instead of wall deformation, although it might not accurately reflect artery wall compliance. This simplification, nonetheless, might impact the precision of the predictions, particularly when there are notable deformations or interactions between blood flow and the elasticity of the vessels. Future research could explore the incorporation of wall compliance into the model to offer a more comprehensive understanding of vascular dynamics. A constant outlet pressure boundary condition of 1 atm (gauge pressure = 0 Pa) [20] was adopted, as is standard practice in computer investigations attempting to separate the effects of geometry and flow behaviour. This simplification eliminates additional uncertainty caused by patient-specific systolic and diastolic pressures, allowing for reliable comparisons across various artery geometries, particularly between idealized and patient-specific models. Second-order upwind methods for pressure and momentum spatial discretisation, a pressure-based solver with a linked scheme for velocity-pressure coupling, and a second-order implicit scheme for the transient formulation of the Navier-Stokes equations were used. The pressure and momentum under-relaxation coefficients were set at 0.25 [1]. To ensure the consistency of the solution, three cardiac cycles were carried out with a constant time-step size of 0.001 and 150 time steps per cardiac cycle [38]. The target convergence criterion was set at 1×10^{-5} for fine convergence.

3. RESULTS AND DISCUSSION

3.1 Flow Patterns in Patient-Specific Femoral Artery

The flow patterns were compared between the healthy idealized femoral artery and the contralateral patient-specific femoral artery. Analysis and comparison were conducted between velocity profiles, pressure distributions, and wall shear stress contours.

3.1.1 Comparison of velocity and pressure distribution in healthy models

Figure 4 shows four key points along the femoral artery that were analyzed in both healthy and patient-specific model simulations. These points are: the upstream region (P1), about 30 mm from the inlet; (P2), around 7 mm before the bifurcation; (P3), 33 mm downstream from the bifurcation; and (P4), approximately 64 mm beyond the bifurcation. The velocity (V/V_o) and pressure (P/P_o) distribution is shown in Figures 5(a) and 5(b) along the centerline of both healthy and patient-specific peripheral artery models, focusing on four key locations (P1 – P4) during the mean inlet velocity. Here, V_o and P_o represent the reference velocity and pressure at the artery's inlet, providing a non-dimensionalized framework for comparing the hemodynamic behavior across different models and locations.

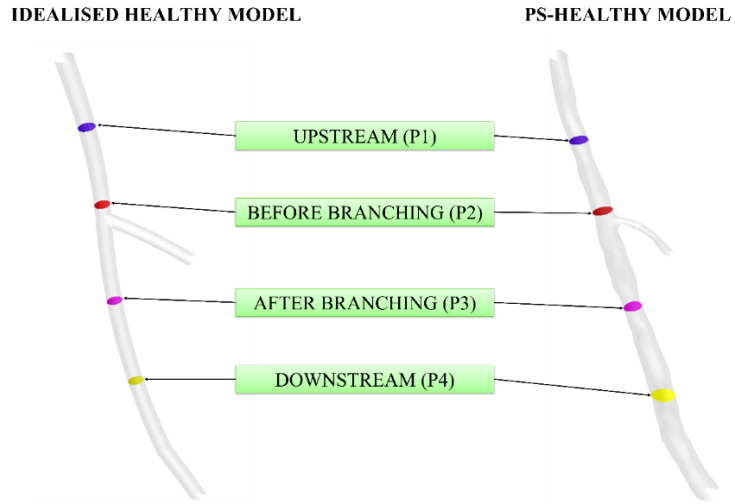

Figure 4. Four primary study locations in (left) the healthy idealized femoral artery model and (right) the contralateral patient-specific femoral artery

The velocity distribution, represented as V/V_o, is normalized against the inlet velocity V_o, which allows for a dimensionless comparison of velocity variations along the arterial centerline. Both models exhibit the highest velocity at the bifurcation point (P2), where the arterial diameter reduces significantly due to the branching of the SFA and profunda. The idealized model achieves a peak velocity of 1.18 m/s V_o at P2, while the patient-specific model peaks at 0.97 m/s V_o, indicating the highest percentage difference of approximately 21%. The idealized model's higher velocity is attributed to its smooth geometry, which minimizes flow resistance. In contrast, the complex geometry of the patient-specific model introduces additional flow disturbances and energy losses, resulting in lower velocities. Downstream of the bifurcation (P3 and P4), both models show a decline in velocity due to the increase in cross-sectional area, which allows for a redistribution of flow. The trends reflect the balance between geometrical constraints and the conservation of mass.

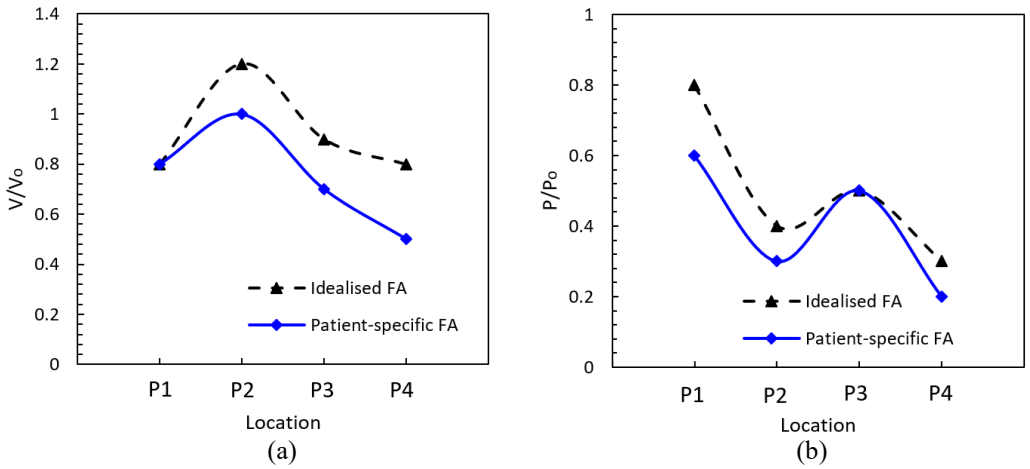

Figure 5. Comparison of (a) velocity and (b) pressure at the centerline of femoral artery between the idealized and patient-specific healthy models

The pressure distribution, represented as P/P_o, is normalized against the inlet pressure P_o, providing a clear comparison of pressure variations along the arterial centerline. Both models show a significant pressure drop after the bifurcation (P2), consistent with the velocity increase observed in Figure 5. This inverse relationship is consistent with Bernoulli's principle, which states that pressure decreases as fluid velocity increases. The idealized model maintains slightly higher pressures than the patient-specific model, particularly in the post-bifurcation regions (P2 and P3). This difference is due to the streamlined geometry of the idealized model, which minimizes flow separation. On the other hand, the patient-specific model's irregularities in anatomy cause kinetic energy losses and increased resistance, which lower pressures. Healthy peripheral artery blood flow is primarily laminar, indicating the flow is smooth and unidirectional. Even in laminar flow conditions, physiological characteristics like sharp bends or bifurcations can create recirculation zones and flow separation. The sudden velocity increase and pressure drop at P2 demonstrate that such phenomena take place in a critical region created by the bifurcation of the SFA and profunda. The lower velocity and pressure observed in the patient-specific model indicate higher energy losses, which are clinically relevant. Abnormal wall shear stress in these areas could put the artery at risk for diseases like thrombosis or atherosclerosis. The energy distribution along the artery becomes affected by geometrical variations, as demonstrated by the normalised pressure values. As the fluid accelerates through the smaller cross-sectional area, the energy conversion from pressure to velocity is highlighted by the abrupt drop in pressure at P2.

3.1.2 Comparison of wall shear stress in healthy models

Wall shear stress (WSS) plays a role in the development of vascular diseases; a study indicates that the development of atherosclerosis plaques can result from low or oscillatory WSS. Assuming laminar flow, the WSS distribution is uniform and symmetric in a mimicked healthy peripheral artery. However, in a patient-specific model, the WSS distribution is more complex and varies due to individual arterial geometry and existing pathologies [19], [26], [49]. During transient flow conditions, such as exercise, WSS can change significantly. In idealized models, WSS may increase and become less uniform due to higher flow rates. In patient-specific models, WSS variability increases with changes in artery shape and pathology [50]-[51]. Figure 6 shows the WSS contour in an idealized healthy femoral artery from 0.05 to 0.75 seconds, while Figure 7 shows the WSS contour in a patient-specific healthy FA. Both models display a significant increase in WSS at the bifurcation area, particularly at P2, which worsens over time. WSS at points P1, P3, and P4 remains more uniform [50].

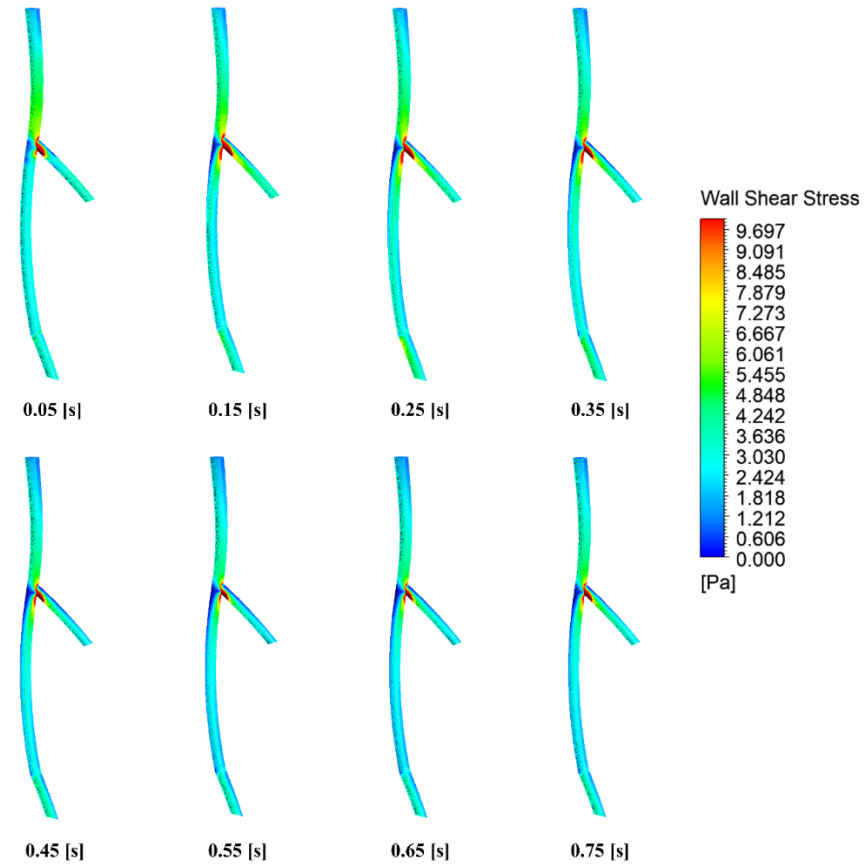

Figure 6. Comparison of WSS obtained for idealized healthy models at different timesteps

The time evolution of mean WSS is illustrated in Figure 8. Overall, mean WSS trends at locations P1, P2, P3, and P4 are similar for both the idealized healthy and the patient-specific healthy FA. Mean WSS was calculated for all cases due to the non-uniform flow caused by complex geometry and curvature. However, the idealized healthy FA shows higher WSS values at P3, likely due to slight differences in the size and bending angle of the profunda in both models [20]. In

contrast, at P2 and P4, the patient-specific healthy FA has a higher WSS distribution because of its more curved and irregular surface compared to the idealized healthy FA.

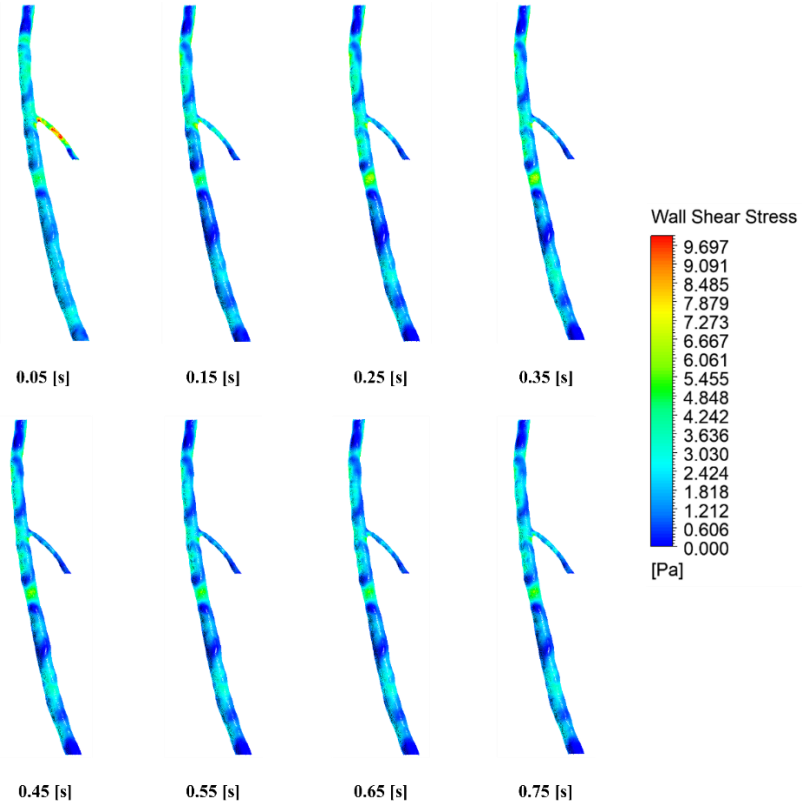

Figure 7. Comparison of WSS obtained for patient-specific healthy models at different timesteps

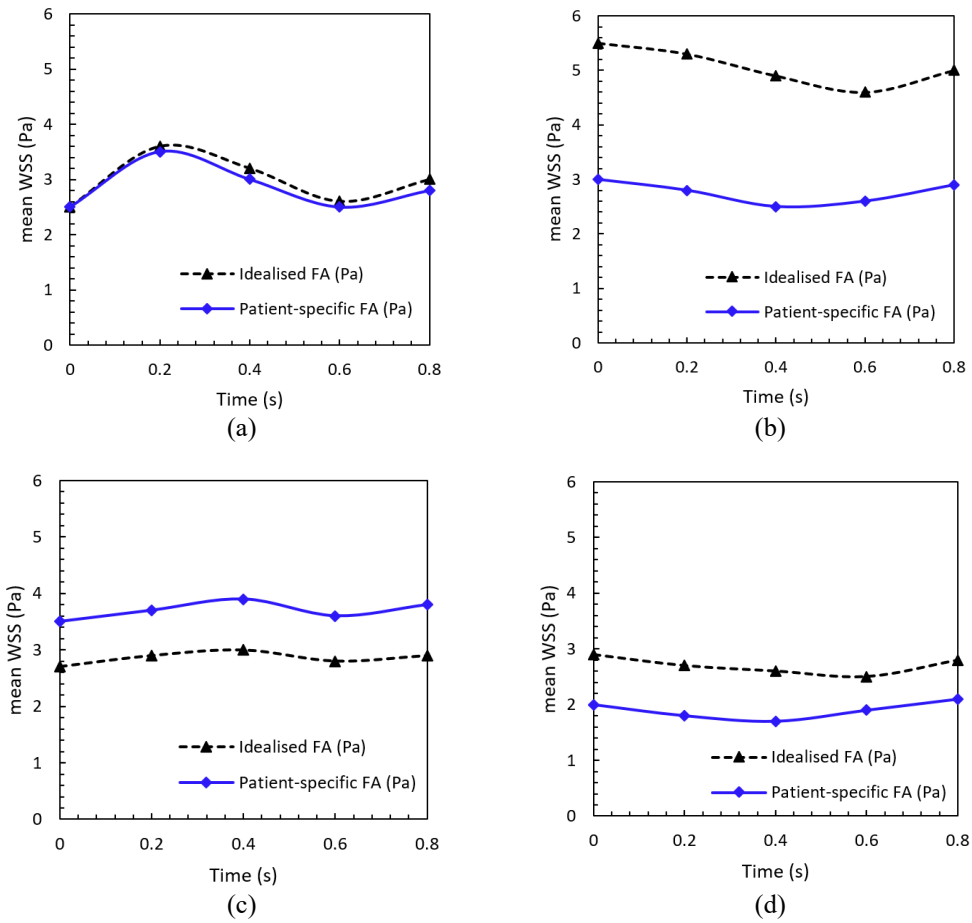

Figure 8. Mean WSS time evolutions at P1-P4 (a)-(d) in patient-specific and idealized FA healthy models

The WSS distribution shows significantly different values but follows a similar trend in both models. The patient-specific model has higher WSS in curved areas and lower WSS where stenosis is likely. This variation is important because low WSS at bifurcations may promote the presence of atherosclerosis. Endothelial cells are more prone to dysfunction due to disturbed blood flow and decreased WSS, which can result in inflammation and the development of plaque [52]. This risk is increased by the irregular blood pressure and flow in these areas.

The hemodynamic effects of arterial pathologies on WSS and the risk of developing arterial diseases have been demonstrated by comparing the WSS of idealized and patient-specific FA models. The findings also demonstrate how the idealized healthy model influences blood flow dynamics by simplifying the artery into a circular cross-section with smooth walls and angular bifurcations. The reconstruction from the femoral to the tibial artery becomes challenging due to the patient-specific model's constantly varying diameter. The idealized model, on the other hand, highlights a significant distinction by employing a fixed diameter for each artery section. There is a significant difference between the profunda and SFA bifurcation areas. The patient-specific model adopts consideration of complex geometries, such as curvature and different cross-sectional diameters, while the idealized model treats profunda as a straight tube and assumes a straightforward angular orientation. The idealized femoral artery model is generally reliable [53] but the CFD results show it performs less accurately in areas with complex geometry, such as irregular shapes and small-radius curves [54]-[55] Despite these drawbacks, the idealized model and the patient-specific model acknowledged relatively well, with maximum errors of 15.8% for wall shear stress, 10% for pressure, and 18% for velocity. Therefore, in order to assess the impact of various stenosis locations on hemodynamic parameters, patient-specific models were used in further simulation.

3.2 Effect of Different Stenosis Locations on Flow Parameters

In this section, the effect of peripheral stenosis on blood hemodynamics was analysed according to the three distinct locations: profunda, proximal to the adductor canal, and mid-superficial femoral artery. The CFD results on flow characteristics, i.e., velocity distribution, WSS, and velocity streamlines corresponding to different stenosis locations, are elaborated in this section.

3.2.1 Velocity distribution in patient-specific arteries at various stenosis locations

Different stenosis locations can lead to different velocity distributions due to the altered anatomy of the wall and blood flow patterns in the femoral artery. The cross-sectional axial velocity distribution for the three stenosis cases: mid-superficial femoral artery (L1), proximal to the adductor canal (L2), and profunda (L3), is shown in Figure 9. According to the findings, L1's maximum velocity was 3.9 m/s, whereas L2's and L3's were 2.8 m/s and 0.9 m/s, respectively. Following stenosis at L1, the flow exhibits irregular and chaotic flows. The difference arises from upstream stenosis, which causes complicated flow patterns that interfere with normal blood flow recovery, particularly when branching vessels occur downstream [56].

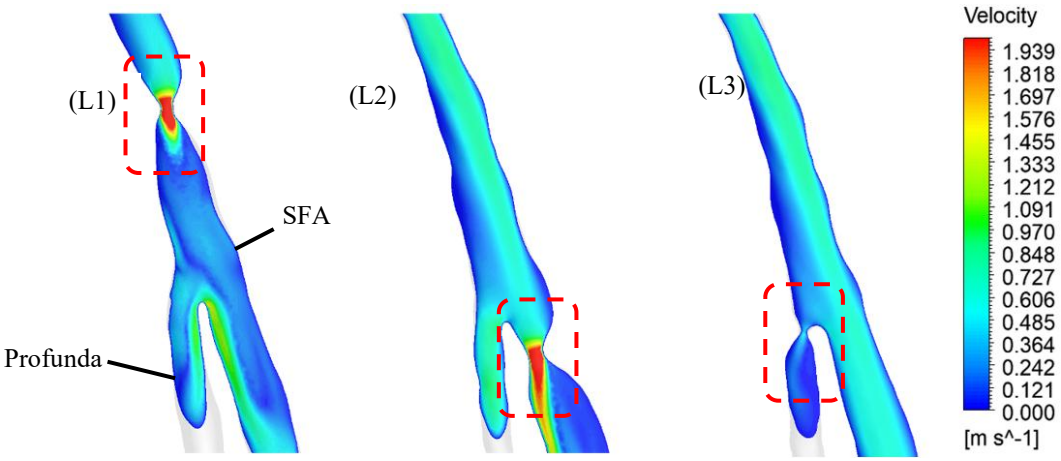

Figure 9. Comparison of the velocity distribution along the midplane of the patient's particular artery for three distinct stenosis locations (L1–L3)

Compared to L1, the flow appears less disturbed in L2 and L3 conditions. Blood flows relatively freely through the main artery, with the branching artery receiving a smaller share of the total flow. This suggests that stenosis in L3 does not significantly affect the main artery's ability to supply blood to the lower extremity. Moreover, the recovery zone in L2 is larger than in L1, where flow velocity normalizes after the stenosis. In summary, while stenosis in any part of a femoral artery can impact blood flow, L1 has a greater effect on velocity distribution due to significant changes in flow characteristics and disturbances from the stenosis.

As seen in Figure 10, stenosis in a femoral artery disrupts normal flow patterns. All three cases show disturbances at the bifurcation area with separation flow and recirculation zones. Stenosis introduces secondary flows like vortices and helical motions. Notably, L1 exhibits significant flow disturbance with separation flow creating secondary streamlines, with Reynolds numbers of 752 at the Profunda's cross-sectional area and 1272 in the mainstream region. Similar low-

Reynolds flow disturbance conditions are observed in the region [57]. In contrast, L2 shows flow disturbances primarily downstream of the bifurcation in the main artery, with a Reynolds number of 1835. Smooth laminar flow is recorded in the profunda. For L3, flow does not show noticeable disturbance, with Reynolds numbers below 1000 in both the profunda and main artery. Stenosis at the upstream region exacerbates flow behavior after the stenosis, hindering full recovery before the profunda branching, disrupting flow streamlines [58].

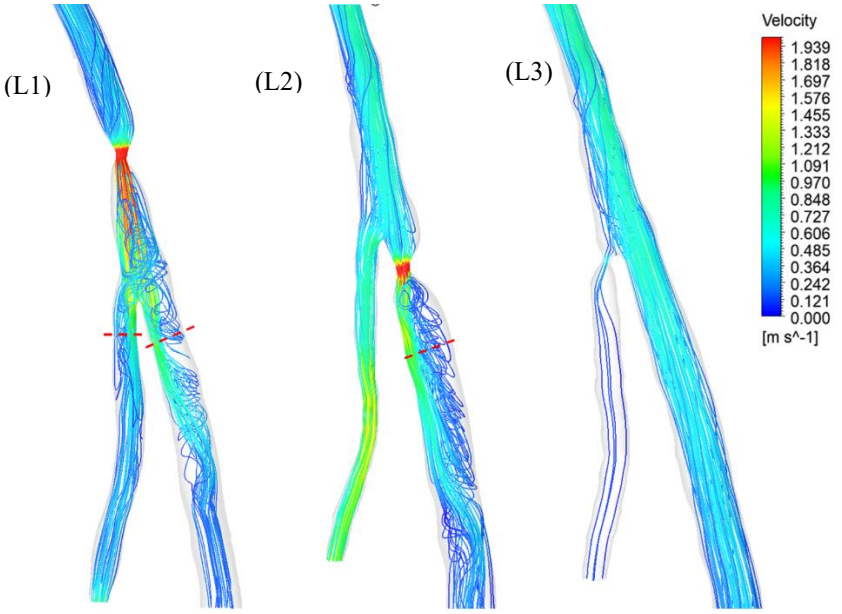

Figure 10. Comparison flow streamlines with the presence of stenosis at three different locations on patient-specific arteries

3.2.2 Wall shear stress distribution at different stenosis locations in patient-specific artery

The complex flow patterns induced by stenosis at different locations may cause differences in WSS along the vessel wall. WSS at L1, L2, and L3 is shown in the WSS contour diagram in Figure 11 below. L1 exhibited the highest WSS of 29 Pa around the throat of the stenosis. The stenotic area in all three locations showed elevated WSS values due to significant flow disturbance. As blood flows beyond the stenosis, WSS gradually recovers toward a more laminar pattern. However, full WSS recovery is not achieved for L1 and L2 [49]. In L1, disturbed and turbulent flow patterns result in regions of low and oscillatory WSS. Conversely, stenosis at L2 also causes flow disturbances but has a lesser impact on the main artery flow. The main artery maintains a relatively stable flow, allowing some recovery of WSS downstream of the stenosis. This contrasts with smaller arteries like the profunda, where stenosis has less influence on overall blood flow.

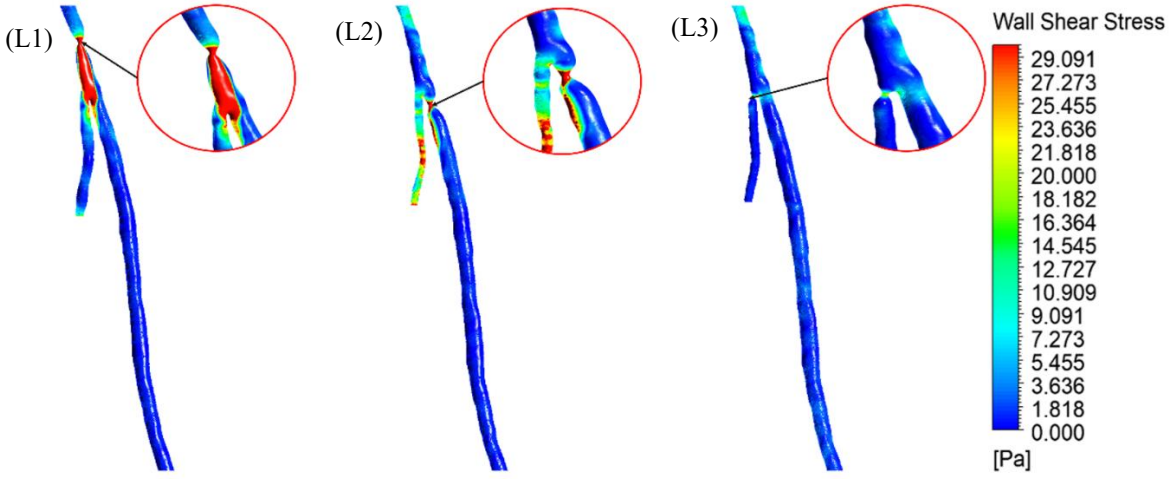

Figure 11. Comparison of WSS distribution for three different stenosis locations along the midplane of patient-specific artery

L1 significantly affects wall shear stress due to disrupted flow patterns and disturbed flow regions. While stenosis at L2 and L3 also causes hemodynamic changes, these effects are less severe as the main artery can sustain a significant portion of blood flow [59]. This study's findings are consistent with clinical research, highlighting that upstream stenosis has a more pronounced effect on blood flow in the femoral artery compared to downstream and profunda stenosis[57],

[60]. Upstream stenosis leads to increased flow velocity due to the stenosis itself, resulting in high-velocity jets, localized turbulence profile, and recirculation zones downstream. These disturbances are worsened at the artery's branching due to incomplete flow recovery [58]. Low-Re turbulence profile and recirculation associated with these flow patterns can produce oscillatory and low WSS areas, which are known to encourage atherosclerosis and endothelial dysfunction [50]. Flow streamline patterns correlate with flow velocity and WSS findings, showing compressed and tightly packed streamlines approaching the stenosis area in cases of upstream stenosis, causing abrupt changes in flow direction and patterns [57], [60].

Furthermore, upstream stenosis is clinically significant and commonly leads to more severe disruptions in blood flow [61]. Changes in WSS and flow patterns contribute significantly to the progression of vascular diseases and symptoms in patients. While downstream stenosis also affects blood flow and WSS, its impact is generally less severe than that of upstream stenosis. Profunda stenosis remains relevant in clinical contexts as it affects the blood supply to specific muscle groups in the lower extremities.

4. CONCLUSIONS

This study revealed distinct hemodynamic characteristics associated with PAD through comparative CFD simulations using both idealized and patient-specific artery models. Significant velocity gradients were observed at critical bifurcation points such as the SFA and profunda femoris artery, with peak velocities exceeding 1.9 m/s in the stenotic regions. WSS analysis identified localized areas of low WSS near branching zones, which are clinically associated with the initiation and progression of atherosclerotic plaques.

The comparison demonstrated that while idealized models offer a simplified platform for preliminary investigations, they fall short in replicating complex flow disturbances introduced by patient-specific anatomical variations. The incorporation of realistic geometries, particularly in stenosed models, is essential to accurately capture disturbed flow patterns, transitional behavior, and high-risk regions, thereby enhancing diagnostic fidelity. These findings provide valuable insights for clinicians by pinpointing hemodynamic markers that may indicate disease progression or treatment efficacy. CFD can thus support personalized treatment planning by enabling non-invasive preoperative assessment, simulation of intervention outcomes, and identification of optimal treatment sites. Future work should focus on integrating patient-specific inlet waveforms, fluid-structure interaction (FSI), and longitudinal clinical data to further enhance predictive capability and clinical utility in the management of PAD.

ACKNOWLEDGEMENTS

The authors would like to thank the Ministry of Higher Education for providing financial support under the Fundamental Research Grant Scheme FRGS/1/2021/TK0/UMP/02/8 (RDU210109).

CONFLICT OF INTEREST

All authors declare that they have no conflicts of interest that are relevant to the content of this article.

AUTHORS' CONTRIBUTION

UZ Shahrulakmar and C Nadarajan conducted the modeling analysis and prepared the initial draft of the manuscript. NH Johari and B Guo reviewed and revised the manuscript for intellectual content. All authors contributed to the final version, read, and approved the manuscript for submission.

REFERENCES

[1] M. Colombo, M. Bologna, M. Garbey, S. Berceli, Y. He, J. F. M. Rodriguez, et al., "Computing patient-specific hemodynamics in stented femoral artery models obtained from computed tomography using a validated 3D reconstruction method," *Medical Engineering & Physics*, vol. 75, pp. 23–35, 2020.

[2] A. Corti, C. Chiastra, M. Colombo, M. Garbey, F. Migliavacca, and S. Casarin, "A fully coupled computational fluid dynamics – agent-based model of atherosclerotic plaque development: Multiscale modeling framework and parameter sensitivity analysis," *Computers in Biology and Medicine*, vol. 118, p. 103623, 2020.

[3] S. Prasertcharoensuk, K. Prateepphuangrat, P. Angkasith, P. Teeratakulpisarn, P. Tanmit, S. Chimluang, et al., "Risk factors of major lower limb amputation in symptomatic peripheral artery disease: A retrospective cohort study," *Future Science OA*, vol. 11, no. 1, p. 2476881, 2025.

[4] R. L. Morley, A. Sharma, A. D. Horsch, and R. J. Hinchliffe, "Peripheral artery disease," *BMJ (Online)*, vol. 360, pp. 1–8, 2018.

[5] A. Rerkasem, A. Mangklabruks, S. Buranapin, K. Sony, N. Inpankaew, R. Rerkasem, et al., "Incidence and predictors of cardiovascular disease mortality and all-cause mortality in patients with type II diabetes with peripheral arterial disease," *PLoS One*, vol. 20, no. 5, p. e0322502, 2025.

[6] A. Gogineni and T. S. Ravigururajan, "Flow dynamics and wall shear stresses in a bifurcated femoral artery," *Journal of Biomedical Engineering and Medical Devices*, vol. 2, no. 2, p. 1000130, 2017.

[7] N. H. Johari, N. B. Wood, Z. Cheng, R. Torii, M. Oishi, M. Oshima, et al., "Disturbed flow in a stenosed carotid artery bifurcation: comparison of RANS-based transitional model and LES with experimental measurements," *International Journal of Applied Mechanics*, vol. 11, no. 4, pp. 1–21, 2019.

[8] S. C. Y. Lo, J. W. S. McCullough, X. Xue, and P. V. Coveney, "Uncertainty quantification of the impact of peripheral arterial disease on abdominal aortic aneurysms in blood flow simulations," *Journal of the Royal Society Interface*, vol. 21, no. 213, p. 20230656, 2024.

[9] Z. Sun, "Diagnostic accuracy of multislice CT angiography in peripheral arterial disease," *Journal of Vascular and Interventional Radiology*, vol. 17, no. 12, pp. 1915–1921, 2006.

[10] R. L. Hewlin and J. P. Kizito, "Development of an experimental and digital cardiovascular arterial model for transient hemodynamic and postural change studies: 'A preliminary framework analysis,'" *Cardiovascular Engineering and Technology*, vol. 9, no. 1, pp. 1-31, 2018.

[11] O. Kawarada, K. Hozawa, K. Zen, H. L. Huang, S. H. Kim, D. Choi, et al., "Peak systolic velocity ratio derived from quantitative vessel analysis for restenosis after femoropopliteal intervention: A multidisciplinary review from Endovascular Asia," *Cardiovascular Intervention and Therapeutics*, vol. 35, no. 1, pp. 52–61, 2020.

[12] A. J. Miller, E. A. Takahashi, W. S. Harmsen, K. C. Mara, and S. Misra, "Treatment of superficial femoral artery restenosis," *Journal of Vascular and Interventional Radiology*, vol. 28, no. 12, pp. 1681–1686, 2017.

[13] M. K. Razavi, D. P. T. Flanigan, S. M. White, and T. B. Rice, "A real-time blood flow measurement device for patients with peripheral artery disease," *Journal of Vascular and Interventional Radiology*, vol. 32, no. 3, pp. 453–458, 2021.

[14] H. E. Salman and Y. Yazicioglu, "Computational analysis for non-invasive detection of stenosis in peripheral arteries," *Medical Engineering & Physics*, vol. 70, pp. 39–50, 2019.

[15] C. Carallo, C. Tripolino, M. S. de Franceschi, C. Irace, X. Y. Xu, and A. Gnasso, "Carotid endothelial shear stress reduction with aging is associated with plaque development in twelve years," *Atherosclerosis*, vol. 251, pp. 63–69, 2016.

[16] A. Desyatova, J. Mactaggart, R. Romarowski, W. Poulson, M. Conti, and A. Kamenskiy, "Effect of aging on mechanical stresses, deformations, and hemodynamics in human femoropopliteal artery due to limb flexion," *Biomechanics and Modeling in Mechanobiology*, vol. 17, no. 1, pp. 181–189, 2018.

[17] N. H. Johari, M. Hamady, and X. Y. Xu, "A computational study of the effect of stent design on local hemodynamic factors at the carotid artery bifurcation," *Artery Research*, vol. 26, no. 3, pp. 161–169, 2020.

[18] S. Schumann, C. Gökgöl, N. Diehm, P. Büchler, and G. Zheng, "Effect of stent implantation on the deformations of the superficial femoral artery and popliteal artery: In vivo three-dimensional deformational analysis from two-dimensional radiographs," *Journal of Vascular and Interventional Radiology*, vol. 28, no. 1, pp. 142–146, 2017.

[19] P. Xu, X. Liu, Q. Song, G. Chen, D. Wang, H. Zhang, et al., "Patient-specific structural effects on hemodynamics in the ischemic lower limb artery," *Scientific Reports*, vol. 6, no. 1, p. 39225, 2016.

[20] C. Gökgöl, N. Diehm, L. Räber, and P. Büchler, "Prediction of restenosis based on hemodynamical markers in revascularized femoro-popliteal arteries during leg flexion," *Biomechanics and Modeling in Mechanobiology*, vol. 18, no. 6, pp. 1883–1893, 2019.

[21] C. Gökgöl, S. Schumann, N. Diehm, G. Zheng, and P. Büchler, "In vivo quantification of the deformations of the femoropopliteal segment," *Journal of Endovascular Therapy*, vol. 24, no. 1, pp. 27–34, 2017.

[22] J. MacTaggart, W. Poulson, A. Seas, P. Deegan, C. Lomneth, A. Desyatova, et al., "Stent design affects femoropopliteal artery deformation," *Annals of Surgery*, vol. 270, no. 1, pp. 180–187, 2019.

[23] M. Colombo, G. Luraghi, L. Cestariolo, M. Ravasi, A. Airoldi, C. Chiastra, et al., "Impact of lower limb movement on the hemodynamics of femoropopliteal arteries: A computational study," *Medical Engineering & Physics*, vol. 81, pp. 105–117, 2020.

[24] X. Li, X. Liu, X. Li, L. Xu, X. Chen, and F. Liang, "Tortuosity of the superficial femoral artery and its influence on blood flow patterns and risk of atherosclerosis," *Biomechanics and Modeling in Mechanobiology*, vol. 18, no. 4, pp. 883–896, 2019.

[25] N. B. Wood, S. Z. Zhao, A. Zambanini, M. Jackson, W. Gedroyc, S. A. Thom, et al., "Curvature and tortuosity of the superficial femoral artery: A possible risk factor for peripheral arterial disease," *Journal of Applied Physiology*, vol. 101, no. 5, pp. 1412–1418, 2006.

[26] D. Wang, F. Serracino-Inglott, and J. Feng, "Numerical simulations of patient-specific models with multiple plaques in human peripheral artery: a fluid-structure interaction analysis," *Biomechanics and Modeling in Mechanobiology*, vol. 20, no. 1, pp. 255–265, 2021.

[27] A. Vink, A. H. Schoneveld, C. Borst, and G. Pasterkamp, "The contribution of plaque and arterial remodeling to de novo atherosclerotic luminal narrowing in the femoral artery," *Journal of Vascular Surgery*, vol. 36, no. 6, pp. 1194–1197, 2002.

[28] D. Lopes, H. Puga, J. Teixeira, and R. Lima, "Blood flow simulations in patient-specific geometries of the carotid artery: A systematic review," *Journal of Biomechanics*, vol. 111, p. 110019, 2020.

[29] N. Filipovic, Z. Teng, M. Radovic, I. Saveljic, D. Fotiadis, and O. Parodi, "Computer simulation of three-dimensional plaque formation and progression in the carotid artery," *Medical & Biological Engineering & Computing*, vol. 51, no. 6, pp. 607–616, 2013.

[30] N. Filipovic, Z. Milosevic, I. Saveljic, D. Nikolic, and M. Radovic, "Computer modeling of stent deployment in the coronary artery coupled with plaque progression," in *Biomaterials in Clinical Practice*, F. Zivic, S. Affatato, S., M. Trajanovic, M. Schnabelrauch, N. Grujovic, K. Choy, Eds. Springer, Cham, pp. 659-693, 2017.

[31] Á. Üveges, C. Jenei, T. Kiss, Z. Szegedi, B. Tar, G. T. Szabó, et al., "Three-dimensional evaluation of the spatial morphology of stented coronary artery segments in relation to restenosis," *International Journal of Cardiovascular Imaging*, vol. 35, no. 10, pp. 1755–1763, 2019.

[32] M. Radovic, V. Isailovic, I. Saveljic, Z. Milosevic, D. Nikolic, T. Exarchos, *et al.*, "Computational modeling of plaque progression in coronary arteries," in *2015 IEEE 15th International Conference on Bioinformatics and Bioengineering (BIBE)*, pp. 1–5, 2015.

[33] N. Ali, A. Zaman, M. Sajid, J. J. Nieto, and A. Torres, "Unsteady non-Newtonian blood flow through a tapered overlapping stenosed catheterized vessel," *Mathematical Biosciences*, vol. 269, pp. 94–103, 2015.

[34] U. Z. Shahrulakmar, N. H. Johari, J. Haron, C. Nadarajan, and M. N. Omar, "Prediction of atherosclerosis in peripheral arterial disease using computational fluid dynamics modelling," in *Proceedings of the 2nd Human Engineering Symposium*, M. H. A. Hassan, M. N. Omar, N. H. Johari, and Y. Zhong, Eds., Singapore: Springer Nature Singapore, pp. 223–237, 2024.

[35] F. P. P. Tan, A. Borghi, R. H. Mohiaddin, N. B. Wood, S. Thom, and X. Y. Xu, "Analysis of flow patterns in a patient-specific thoracic aortic aneurysm model," *Computers & Structures*, vol. 87, pp. 680–690, 2009.

[36] T. A. Spirka, J. G. Myers, R. M. Setser, S. S. Halliburton, R. D. White, and G. P. Chatzimavroudis, "Construction of a computational non-planar curved tube model from MRI data," in *IEEE International Workshop on Imaging Systems and Techniques 2005*, pp. 79–82, 2005.

[37] C. Gökgöl, Y. Ueki, D. Abler, N. Diehm, R. P. Engelberger, T. Otsuka, et al., "Towards a better understanding of the posttreatment hemodynamic behaviors in femoropopliteal arteries through personalized computational models based on OCT images," *Scientific Reports*, vol. 11, no. 1, pp. 1–12, 2021.

[38] A. Ferrarini, A. Finotello, G. Salsano, F. Auricchio, D. Palombo, G. Spinella, et al., "Impact of leg bending in the patient-specific computational fluid dynamics of popliteal stenting," *Acta Mechanica Sinica/Lixue Xuebao*, vol. 37, no. 2, pp. 279–291, 2021.

[39] F. Donadoni, M. Bonfanti, C. Pichardo-Almarza, S. Homer-Vanniasinkam, A. Dardik, and V. Díaz-Zuccarini, "An in silico study of the influence of vessel wall deformation on neointimal hyperplasia progression in peripheral bypass grafts," *Medical Engineering & Physics*, vol. 74, pp. 137–145, 2019.

[40] H. Liu, L. Lan, J. Abrigo, H. L. Ip, Y. Soo, D. Zheng, et al., "Comparison of Newtonian and non-newtonian fluid models in blood flow simulation in patients with intracranial arterial stenosis," *Frontiers in Physiology*, vol. 12, pp. 1–11, 2021.

[41] A. F. Totorean, I. C. Totorean, S. I. Bernad, T. Ciocan, D. C. Malita, D. Gaita, et al., "Patient-specific image-based computational fluid dynamics analysis of abdominal aorta and branches," *Journal of Personalized Medicine*, vol. 12, no. 9, p. 5502, 2022.

[42] M. G. Al-Azawy, S. K. Kadhim, and A. S. Hameed, "Newtonian and non-newtonian blood rheology inside a model of stenosis," *CFD Letters*, vol. 12, no. 11, pp. 27–36, 2020.

[43] M. S. Olufsen, C. S. Peskin, W. Y. Kim, E. M. Pedersen, A. Nadim, and J. Larsen, "Numerical simulation and experimental validation of blood flow in arteries with structured-tree outflow conditions," *Annals of biomedical engineering*, vol. 28, no. 11, pp. 1281–1299, 2000.

[44] U. Z. Shahrulakmar, N. H. Johari, M. F. M. Fauzi, J. Haron, C. Nadarajan, and M. N. Omar, "Numerical approach for the evaluation of hemodynamic behaviour in peripheral arterial disease: A systematic review," *Journal of Advanced Research in Fluid Mechanics and Thermal Sciences*, vol. 103, no. 2, pp. 95–117, 2023.

[45] F. P. P. Tan, N. B. Wood, G. Tabor, and X. Y. Xu, "Comparison of les of steady transitional flow in an idealized stenosed axisymmetric artery model with a RANS transitional model," *Journal of Biomechanical Engineering*, vol. 133, no. 5, pp. 1–12, 2011.

[46] S. A. Ahmed and D. P. Giddens, "Pulsatile poststenotic flow studies with laser Doppler anemometry," *Journal of Biomechanics*, vol. 17, no. 9, pp. 695–705, 1984.

[47] M. S. Olufsen, C. S. Peskin, W. Y. Kim, E. M. Pedersen, A. Nadim, and J. Larsen, "Numerical simulation and experimental validation of blood flow in arteries with structured-tree outflow conditions," vol. 28, pp. 1281–1299, 2000.

[48] N. H. Johari, M. Hamady, and X. Y. Xu, "Fluid-structure interaction study of the effect of stent on local hemodynamics parameters at the stented carotid artery bifurcation," *Journal of Advanced Research in Applied Sciences and Engineering Technology*, vol. 28, no. 2, pp. 247–255, 2022.

[49] U. Z. Shahrulakmar, M. N. Omar, and N. H. Johari, "Brief review on recent advancement of computational analysis on hemodynamics in peripheral artery disease," in *Technological Advancement in Instrumentation & Human Engineering, Lecture Notes in Electrical Engineering*, pp. 555–572, 2023.

[50] M. Zhou, Y. Yu, R. Chen, X. Liu, Y. Hu, Z. Ma, L. Gao, et al., "Wall shear stress and its role in atherosclerosis," *Frontiers in Cardiovascular Medicine*, vol. 10, pp. 1–11, 2023.

[51] A. F. H. M. Noor, N. H. Johari, A. A. Basri, and X. Y. Xu, "Comparison of velocity profiles in stented carotid artery bifurcation between computational fluid dynamics and particle image velocimetry measurements," *International Journal of Automotive and Mechanical Engineering*, vol. 21, no. 2, pp. 11386–11397, 2024.

[52] S. Jebari-Benslaiman, U. Galicia-García, A. Larrea-Sebal, J. R. Olaetxea, I. Alloza, K. Vandenbroeck, et al., "Pathophysiology of Atherosclerosis," *International Journal of Molecular Sciences*, vol. 23, no. 6, p. 3346, 2022.

[53] D. Afkari and F. Gabaldón, "Fluid-solid interaction in arteries incorporating the autoregulation concept in boundary conditions," *Computer Methods in BiomeChaniCs and BiomediCal Engineering*, vol. 19, no. 9, pp. 985–1001, 2016.

[54] V. Peiffer, S. J. Sherwin, and P. D. Weinberg, "Computation in the rabbit aorta of a new metric – the transverse wall shear stress – to quantify the multidirectional character of disturbed blood flow," *Journal of Biomechanics*, vol. 46, no. 15, pp. 2651–2658, 2013.

[55] P. J. Blanco, S. M. Watanabe, M. A. R. F. Passos, P. A. Lemos, and R. A. Feijóo, "An anatomically detailed arterial network model for one-dimensional computational hemodynamics," *IEEE Transactions on Biomedical Engineering*, vol. 62, no. 2, pp. 736–753, 2015.

[56] N. Mustapha, P. K. Mandal, P. R. Johnston, and N. Amin, "A numerical simulation of unsteady blood flow through multi-irregular arterial stenoses," *Applied Mathematical Modelling*, vol. 34, no. 6, pp. 1559–1573, 2010.

[57] B. Liu, "The influences of stenosis on the downstream flow pattern in curved arteries," *Medical Engineering & Physics*, vol. 29, no. 8, pp. 868–876, 2007.

[58] S. Torii, J. A. Mustapha, J. Narula, H. Mori, F. Saab, H. Jinnouchi, et al., "Histopathologic characterization of peripheral arteries in subjects with abundant risk factors: Correlating imaging with pathology," *JACC: Cardiovascular Imaging*, vol. 12, no. 8, Part 1, pp. 1501–1513, 2019.

[59] M. F. M. Fauzi, N. H. Johari, M. J. M. Mokhtarudin, B. M. Yusoff, and B. Guo, "Fluid-structure interaction modelling of blood flow in peripheral arterial disease," *Journal of Advanced Research in Fluid Mechanics and Thermal Sciences*, vol. 119, no. 1, pp. 117–133, 2024.

[60] N. H. Johari, K. Osman, Z. Mohd Salleh, J. Haron, and M. R. Abdul Kadir, "The effect of different locations of tracheal stenosis to the flow characteristics using reconstructed CT-scanned image," *Journal of Mechanics in Medicine and Biology*, vol. 12, no. 4, pp. 1–15, 2012.

[61] J. I. Weitz, J. Byrne, G. P. Clagett, M. E. Farkouh, J. M. Porter, D. L. Sackett, et al., "Diagnosis and treatment of chronic arterial insufficiency of the lower extremities: A critical review," *Circulation*, vol. 94, no. 11, pp. 3026–3049, 1996.